2000 June 15

VLBA Scientific Memorandum 24: Strategies for Phase Referencing with the VLBA

J. M. Wrobel, R. C. Walker, and J. M. Benson

National Radio Astronomy Observatory,
P.O. Box O, Socorro, New Mexico 87801

jwrobel@nrao.edu, cwalker@nrao.edu, jbenson@nrao.edu

and

A. J. Beasley

National Radio Astronomy Observatory,
520 Edgemont Road, Charlottesville, Virginia 22903

tbeasley@nrao.edu

ABSTRACT

Strategies for phase referencing with the VLBA are recommended. These strategies cover the proposal, observation, and correlation stages.

Subject headings: astrometry – catalogs – radio continuum – techniques: interferometric

1. INTRODUCTION

Phase-referenced observations with the VLBA have two key advantages over pure self-calibration techniques. First, weaker target sources can be observed because the effective coherence time is increased from minutes to hours. This greatly increases the number of target sources available to the VLBA, including, for example, gamma-ray bursts (Taylor et al. 1999b), quiescent radio stars (Beasley & Güdel 2000), Seyfert galaxy nuclei (Wrobel 2000), and sources in selected sky patches (Garrington, Garrett, & Polatidis 1999). Second, the position of the target source can be measured accurately relative to the phase reference source. This permits registration of VLBA images with those from other instruments, as well as registration of VLBA movie frames spanning days to years and yielding, for example, proper motions of pulsars (Fomalont et al. 1999), masers (van Langevelde et al. 1999), or sources in the Galactic Center (Reid et al. 1999). Phase referencing is currently used in 30-50% of VLBA observations. This popularity stems both from the two compelling advantages just mentioned, as well as an end-to-end implementation of phase referencing on the VLBA.

All phase-referenced observations with the VLBA involve a phase calibrator (the *calibrator* hereafter) and a target source (the *target* hereafter). The VLBA supports three styles of phase referencing, commonly called the *nodding style* (Beasley & Conway 1995), the *in-beam style* (Fomalont 1995), and the *spectral-line style* (Reid 1999; Herrnstein et al. 1998). The nodding and in-beam styles involve calibrators and targets that are separate sources, each of which can be a line or continuum source. The spectral-line style involves phase referencing a weak line or continuum target to a strong line feature in the same source, and is not discussed further.

Descriptions of both the nodding and in-beam styles will employ the selected VLBA parameters in Table 1, which follow the notation used by (Wrobel 1999):

Col. 1: Observing frequency ν.

Col. 2: FWHM primary beam Θ_{FWHM} of an antenna.

Col. 3: Recommended switching time τ_s, defined in the following paragrah, for the nodding style.

Col. 4: Recorded bandwidth $\Delta\nu^{128}_{REC}$ for 4-level (2-bit) sampling of a single polarization for recordings at the VLBA's sustainable aggregate bit rate of 128 Mbps.

Col. 5: Fringe-fit interval $\tau_{\rm ff}$ for a calibrator observation, where fringe-fitting means solving for the phase, rate, and delay.

Col. 6: Baseline sensitivity ΔS^{128} for a single polarization in $\tau_{\rm ff}$.

Col. 7: Total integration time $t_{\rm int}$ of the target observations.

Col. 8: Image sensitivity $\Delta I^{128}_{\rm m}$ for a single polarization given $\Delta\nu^{128}_{REC}$ and $t_{\rm int}$.

Col. 9: FWHM synthesized beam θ_{FWHM} of a uniformly-weighted image. A phase-referenced target is often weak and therefore imaged with natural, not uniform, weighting that optimizes image sensitivity but degrades image resolution. However, other weighting schemes can be applied that slightly degrade sensitivity but achieve close to uniform resolution (Briggs, Schwab, & Sramek 1999).

In the nodding style, the array nods between the calibrator and the target, and the correlator processes the observations once. The nodding is characterized by a *switching time* τ_s, defined as the time interval between the center of successive calibrator observations; and by a *switching angle* θ_s, defined as the angular distance between the calibrator and target. The correlator models both the geometry of the array and at least some aspects of the atmosphere above each antenna in the array. Post-processing software is used to calibrate the amplitudes of both calibrator and target observations using traditional techniques. Other software is used to solve for the phase, rate, and delay of each calibrator observation, and then to interpolate those calibrator phases, perhaps assisted by the rates, to derive phases appropriate for the interleaved target observations.

The calibrated complex visibilities from the target observations are then weighted and inverted to yield a synthesis image of the target, as phase referenced to the calibrator. Figure 1 shows a VLBA nodding example at an observing frequency $\nu = 8.4$ GHz (Wrobel 2000). The top panel shows the position of the calibrator J1419+2706 relative to that of the target NGC 5548. These relative positions are greater than the antenna's primary beam Θ_{FWHM} at frequency $\nu = 8.4$ GHz (Table 1, Col. 2), so the array was nodded through the switching angle $\theta_s = 2°$. A switching time of $\tau_s = 300$ s was used, based on a target observation lasting 180 s being bracketed by calibrator observations each lasting 120 s. The calibrator was strong enough to be detected in a 120-s fringe-fit interval given the VLBA baseline sensitivity, which was $\sqrt{2}$ better than that quoted in Column 6 of Table 1 because twice the sustainable recording rate was used. The bottom panel in Figure 1 shows the naturally-weighted synthesis image of the 2-mJy target NGC 5548, as phase referenced to the calibrator J1419+2706.

In the in-beam style, the array simultaneously observes the calibrator and the target because both fit within the primary beam of a VLBA antenna. The correlator processes the observations twice, once at the calibrator position and once at the target position. Subsequent post-processing steps are similar to the nodding style. Figure 2 shows a VLBA in-beam example at an observing frequency $\nu = 0.33$ GHz (Taylor et al. 1999a). The top panel shows the calibrator J1252+5634 position relative to that of the target Mrk 231. These relative positions are less than the antenna's primary beam Θ_{FWHM} at frequency $\nu = 0.33$ GHz (Table 1, Col. 2). Thus both sources were simultaneously observed, effectively reducing the switching time to $\tau_s = 0$ s. However, two correlation passes were needed, one at the position of J1252+5634 and one at the position of Mrk 231, with these two positions defining a switching angle $\theta_s = 36' = 0.6°$. Despite some primary beam attenuation, the calibrator was strong enough to be detected in a 60-s fringe-fit interval given the tabulated VLBA baseline sensitivity (Table 1, Col. 6). The bottom panel shows the synthesis image of the 150-mJy target Mrk 231, as phase referenced to the calibrator J1252+5634.

Strategies for successful phase referencing, as in the examples in Figures 1 and 2, follow from knowing what factors limit phase referencing as implemented on the VLBA. Section 2 briefly describes those limiting factors, emphasizing that the switching angle θ_s is set by angular phase variations, the switching time τ_s for the nodding style is set by temporal phase variations, and the origin of phase variations with both angle and time depend strongly on the observing frequency ν. Section 3 recommends strategies for phase referencing, covering the proposal, observation, and correlation stages. Ulvestad (2000) provides recipes for calibrating phase-referenced observations in AIPS.

The strategies covered in this document typically provide *relative* positions good to a about 1 mas. It is possible to do much better using special observing techniques. For example, geodetic methods plus occasional observations covering the sky can improve the troposphere model. Multiple calibrators surrounding the target can also be used to remove atmospheric gradients. Neither method has been integrated well into the available postprocessing software so they should only be attempted by experienced observers. These methods will not be mentioned further here.

2. LIMITATIONS TO PHASE REFERENCING

2.1. General Remarks

Phase referencing will be limited by model errors remaining after correlation and initial phase calibration, provided those errors depend on direction or time (Walker 1999b). Geometric errors, such as source and antenna positions, will degrade phase-referenced phases by up to the total error times the calibrator-target separation θ_s, expressed in radians. Atmospheric effects, including contributions from both the troposphere and the ionosphere, scale with the secant of the zenith angle z, which can be very different at separate VLBA antennas. Errors in models for the static atmosphere induce errors that scale with the difference in $\sec(z)$ between calibrator and target, and these can become significant at high zenith angles even for small switching angles θ_s. Atmospheric terms can also vary rapidly in both time and space, and such dynamic variations will degrade phase referencing done with either too long a switching time τ_s or too large a switching angle θ_s.

2.2. Geometry and Clocks

A unique atmosphere overlays each antenna and an independent frequency standard, or clock, is used at each antenna. Ignoring the atmosphere and clocks, the geometric model currently used by the VLBA correlator should be good to a few centimeters at worst, which corresponds to less than a few turns of phase across the sky. Beware, however, that the accuracy of the calibrator position used at correlation will limit phase referencing. To first order the calibrator position error will shift the target position by that error. But second-order effects create phase errors that can limit dynamic range. Simulations suggest that a calibrator position error will limit the dynamic range in the phase referenced image, with this limit being about 25 at an observing frequency $\nu = 8.4$ GHz for switching angle $\theta_s = 2°$ and a calibrator position error of 10 mas (Beasley & Conway 1995). Modern clocks themselves are not much of a problem because they do not change with pointing position; their long-term variations can be tracked, and corrected, with calibrator observations; and their short-term variations are generally smaller than the atmospheric variations.

2.3. Atmosphere

The unique atmosphere above each antenna is the dominant source of errors when phase referencing. Thus to estimate when phase referencing can be done and with what parameters, the properties of both the static and the dynamic atmosphere must be understood. Further details can be found in Thompson, Moran, & Swenson (1986), Beasley & Conway (1995), and Sovers et al. (1998).

2.3.1. Static and Dynamic Troposphere

The lower few kilometers of the Earth's atmosphere are known as the troposphere. The phase of a monochromatic radio signal propagating through the troposphere is delayed relative to an equivalent path through a vacuum. The correlator model applies a priori estimates of propagation delays through a static troposphere with two components: a hydrostatic component which depends on the antenna's latitude and height above the geoid, plus the season; and a wet component which depends on the antenna's latitude (Niell 1996). At zenith, the dry troposphere contributes about 2 m of excess path delay, while the wet component can contribute up to about 0.3 m. The propagation delay through the wet troposphere is highly dynamic, however, due to rapid variations in its precipitable water vapor. This motivated Treuhaft & Lanyi (1987) to model the dynamic troposphere as a frozen screen characterized by a rockiness parameter C_n, with the screen located at a scale height $L_t \sim 1 - 2$ km and blowing with speed $v_t \sim 10$ m s^{-1} over each antenna. The correlator model does not apply any a priori estimates of propagation delay through the dynamic troposphere. Correlator model errors are dominated by tropospheric effects at observing frequencies $\nu \geq 5$ GHz.

The correlator model applies a priori estimates of propagation delays through the static troposphere toward the calibrator and the target, separated by a switching angle θ_s. This source pair will be observed at different zenith angles z at each antenna. So errors in the model for the static troposphere induce errors that scale with the difference in $\sec(z)$ between calibrator and target, and these can become especially significant at high zenith angles even for small switching angles θ_s. This leads to two strategies: minimize the switching angle θ_s and avoid high zenith angles z.

The dynamic troposphere can be especially limiting when phase referencing at high observering frequenices ν, and those limitations have been extensively studied (Carilli, Carlstrom, & Holdaway 1999). What has been learned on the VLA about phase fluctuations at high frequencies ν can also be used to understand the VLBA case. This is because although VLBA baseline lengths b always exceed the tropospheric scale height L_t, the longest baselines on the VLA are also longer than that scale height and so should behave similarly. The characterizations of phase differences as a function of baseline length b, the so-called phase structure function with amplitude C_n^2, can be used to understand the differences between the sight-lines to the calibrator and the target, separated by a switching angle θ_s. Those lines of sight diverge from the antenna, but are actually rather close until beyond the tropospheric scale height L_t. For $\theta_s = 5.7^\circ = 0.1$ radian, the lines of sight at the zenith are only 100 m apart at a scale height $L_t = 1$ km. This small spatial separation within the dynamic troposphere means that both sightlines experience the same fluctuating delay; that is, both are within the same isoplanatic patch. There is thus no need to seek a smaller θ_s. But beware that the spatial separation within the dynamic troposphere can become large at high zenith angles.

The dynamic troposphere does strongly constrain the switching time τ_s, however. The structure-function analysis of the fluctuating tropospheric delay (Treuhaft & Lanyi 1987) was used to predict critical switching times (Beasley & Conway 1995). These predictions were based on the require-

ment that the root-mean-square path variations between successive calibrator observations were less than a quarter of the observing wavelength, which should allow phases to be connected, without 2π-ambiguities, 95% of the time. For typical conditions in the dynamic tropospheric, theory predicts that phase referencing at zenith angles $z \leq 60 - 70°$ will succeed with switching times $\tau_s \sim 160 - 440$ s at an observing frequency $\nu = 8.4$ GHz and $\tau_s \sim 25 - 30$ s at $\nu = 43$ GHz (Ulvestad 1999b). Experience verifies that phase referencing does indeed work with $\tau_s = 300$ s at $\nu = 8.4$ GHz (Taylor et al. 1999b; Beasley & Güdel 2000; Wrobel 2000) and with $\tau_s = 30$ s at $\nu = 43$ GHz (Reid et al. 1999).

2.3.2. Static and Dynamic Ionosphere

The uppermost component of the Earth's atmosphere, the ionosphere, is a region of plasma within which the density peaks at a height of about 350 km, but is widely distribued through heights from 80 to 1000 km. The phase of a radio signal propagating through the ionosphere is advanced relative to an equivalent path through a vacuum, while the group delay is retarded. The delay effect depends on the inverse square of the observing frequency ν, and corresponds to a characteristic extra path length of about 2 m at $\nu = 2$ GHz, but can vary by an order of magnitude or more between day and night, and with the solar cycle. By analogy with the tropospere, the propagation effects of the ionosphere can be divided into a static component which is smoothly varying in angle and in time, upon which is superposed a dynamic component with irregularities on many temporal and spatial scales.

Geodetic measurements using the GPS navigation system are subjected to similar propagation effects and are beginning to be used to generate global models of the static ionosphere from day to day, and even within a day (Wilson et al. 1995). These GPS-based modelling techniques, currently primitive, are evolving quickly. Once they have matured sufficiently it may be feasable to use them at the correlator to apply a priori estimates of propagation delays through the static ionosphere (Walker & Chatterjee 1999). In the interim, a GPS-based model can be applied as a calibration step (Ulvestad 2000). A statistical model for the dynamic ionosphere, analagous to the Treuhaft & Lanyi (1987) model for the dynamic troposphere, has not been developed. The correlator model does not apply any a priori estimates of propagation delay through either the static or dynamic ionosphere. This means that correlator model errors are dominated by ionospheric effects at observing frequencies $\nu < 5$ GHz.

Propagation effects in the static ionosphere, as in the static troposphere, scale with $\sec(z)$ at zenith angles smaller than about 80°. At larger zenith angles these effects begin to level off because of the curvature of the Earth and the fact that the main ionospheric effects occur at an altitude of 300-500 km. The delay contribution is large and unmodelled, so the $\sec(z)$ dependence can lead to very large, and problematic, differences between calibrator and target even for a small switching angle θ_s between the pair. This leads to two strategies: minimize the switching angle θ_s and avoid high zenith angles z. The ionosphere is especially problematic at $\nu = 0.33$ and 0.61 GHz, to the

extent that phase referencing in the nodding style is unlikely to succeed. Rather, the preferred approach is the in-beam style which benefits from the large primary beam (Table 1, Col. 2) and the high density of background sources at those frequencies (Fomalont 1995), with the caveat that adequately compact sources are required.

The passage of acoustic-gravity waves through the ionosphere leads to variations in total electon content, thus affecting propagation delay. The most common, and thus most important, of these involve medium-scale travelling ionospheric disturbances. These occur at height $L_i \sim 400$ km with length scales $l_i \sim 40 - 160$ km and speeds $v_i \sim 100 - 200$ m s^{-1} (Perley & Erickson 1984). These traits immediately suggest that observations through a disturbed ionosphere could require switching times τ_s short as $200 - 400$ s and switching angles θ_s as small as 5°. What does experience reveal? Early tests with MERLIN at $\nu = 1.7$ GHz indicated that, in the majority of circumstances, phase referencing would succeed for switching angles $\theta_s \leq 3°$ and switching times $\tau_s \leq 420$ s (Patnaik et al. 1992). At $\nu = 1.4 - 1.7$ GHz, phase referencing with the VLBA has been shown to be possible using a nodding calibrator at $\theta_s \leq 4 - 5°$ and $\tau_s = 300$ s and to be very reliable with an in-beam calibrator (Chatterjee 1999a,b; Fomalont et al. 1999).

For adequately strong sources, the ionosphere can be measured in real time by comparing VLBA delays or, with care, phases measured at two well separated frequencies. For example, Brisken et al. (2000) have demonstrated a new technique, based on simultaneous observations spanning $\nu = 1.4 - 1.7$ GHz, to remove ionospheric effects from nodding observations of strong targets. In addition, special antenna optics allow simultaneous observations at $\nu = 2.3$ and 8.4 GHz. The geodetic community routinely uses such dual-frequency observations to remove the effects of the ionosphere from their geodetic and astrometric observations of strong sources.

3. STRATEGIES FOR PHASE REFERENCING

3.1. Preparing Observing Proposals

3.1.1. Styles of Requested Time

The VLBA accommodates three styles of requested time (fixed, dynamic, and target of opportunity) and each style is compatible with employing phase referencing.

3.1.2. Planning Tools for Targets

The NRAO scheduling software SCHED (Walker 2000) offers a tool to display a target's elevation at each VLBA antenna, useful if the proposer prefers to avoid requesting observations at high zenith angles z. Values of $z \leq 70°$ are commonly adopted for the reasons discussed in Section 2, leading to a request for about 7 elapsed hours for a target at intermediate declinations. That tool can

also display the Sun's celestial position, useful if the proposer prefers to request observations when portions of the VLBA, usually the innermost antennas in the southwestern states, would be used during nighttime. Example plots in black and white from this tool appear in Figure 3. Color versions of such plots can also be made, in which the antennas are distinguished by a color code.

3.1.3. Selecting a Switching Angle θ_s

Figure 4 shows the celestial positions of 2700 *candidate* phase calibrators in the source catalog, dated 2000 April 17, in use at the VLBA correlator and distributed with SCHED. That program can be used to plot which candidate calibrators are close to the celestial position of a target; examples of such right ascension – declination (RD) plots appear in the top panels of Figures 1 and 2. For the reasons emphasized in Section 2, it is generally preferable to select the closest candidate calibrator as the phase calibrator. But this should only be done after confirming that the closest candidate will be adequately strong and compact for VLBA observations. Electronic archives of VLBA and VLBI visibility plots, listed in Table 2 in descending order of size, should be consulted for this purpose. When mining these archives, keep in mind that they contain information on sources that typically vary in strength and structure over time. Source strength issues are discussed in Section 3.1.4.

For the reasons mentioned in Section 2.2, it is prudent to confirm that the positional accuracy of the closest candidate calibrator is adequate to achieve the proposal goals. This accuracy is conveyed visually in the RD plots by symbols and can be quantified by consulting the following references:

Triangle: 601 sources from surveys by the U.S. Naval Observatory (USNO). Positions usually have two-dimensional accuracies better than $\sqrt{2} \times (1 - 2)$ mas (Ma et al. 1998).

Diamond: 1819 sources from the Jodrell-Bank VLA Astrometric Survey (JVAS) and suitable as MERLIN calibrators. Positions have two-dimensional accuracies of 12 mas in the region $35° \leq \delta_{B1950} \leq 75°$ (Patnaik et al. 1992); of 14 mas in the region $0° \leq \delta_{B1950} \leq 20°$ (Browne et al. 1998); and usually of 55 mas elsewhere in the northern sky (Wilkinson et al. 1998).

Square: 280 sources from the VLA Calibrator Manual. Positions have various accuracies and some could be in error by more than 150 mas (Perley & Taylor 1999).

An accurate source position service is administrated by NRAO should an improved position be required for any candidate calibrator plotted as a diamond or square (Walker 1999a). Requests to that service should be made no later than proposal time for positions needed at correlation time. There are now 2700 candidate calibrators in the source catalog. Efforts are under way to improve the JVAS positions through the VLBA Calibrator Survey, to find JVAS-like sources in the northern Galactic Plane, and to add southern JVAS sources. The source catalog will be updated as those efforts are completed.

Those proposing phase referencing in the in-beam style should request two passes with the VLBA correlator, one pass at the position of the target and one pass at the position of the in-beam calibrator. It is best to attempt to identify the in-beam calibrator at the observing proposal stage. Searches through the source catalogs and archives listed above might not yield an appropriate in-beam calibrator, and it may be necessary to obtain a preparatory image of the VLA (= VLBA) primary beam at the observing frequency of interest, or to search source lists from various published sky surveys (Condon 1999). It may be also advantageous to propose a combination of the in-beam and nodding styles, as demonstrated by Fomalont et al. (1999) at observing frequencies $\nu = 1.4 - 1.7$ GHz. The nodding calibrator can be used to extend significantly the solution interval used to detect the in-beam calibrator, which can then be used to remove the effects of phase gradients between the nodding calibrator and the target. This enables the use of rather weak in-beam calibrators.

3.1.4. Selecting a Switching Time τ_s

The switching time τ_s for the nodding style is dominated by the dynamic troposphere at observing frequencies $\nu \geq 5$ GHz and by the dynamic ionosphere at observing frequencies $\nu < 5$ GHz.

At intermediate observing frequencies $\nu = 1.4 - 8.4$ GHz and under typical atmospheric conditions, experience indicates that phase referencing in the nodding style will succeed with $\tau_s = 300$ s (Table 1, Col. 3). This switching time commonly involves a target observation of 180 s, bracketed by calibrator observations each lasting 120 s. The switching time influences calibrator selection, because the calibrator should be detectable with a signal-to-noise ratio much greater than 10 given the recorded bandwidth $\Delta\nu^{128}_{REC}$, fringe-fit interval $\tau_{ff} = 120$ s, and associated baseline sensitivity ΔS^{128} (Table 1, Cols. 4-6). The switching time also influences the total integration time t_{int} on target. For observations confined to 7 elapsed hours, as recommended in Section 3.1.2, about one-half of the time will be spent observing the phase calibrator plus other calibrators (see Section 3.2). This will leave $t_{int} = 3.5$ h on target (Table 1, Col. 7), leading to the expected image sensitivities ΔI^{128}_{m} (Table 1, Col. 8). At observing frequencies $\nu \geq 15$ GHz even shorter switching times must be used: as a rule, τ_s is about twice τ_{ff} (Table 1, Cols. 3, 5), and the poorer antenna performance at these frequencies leads to worse baseline and image sensitivities (Table 1, Col. 6, 8).

At low observing frequencies $\nu = 0.33 - 0.61$ GHz and under typical ionospheric conditions, experience indicates that phase referencing will succeed only in the in-beam style. This effectively reduces the switching time to $\tau_s = 0$ s. For observations confined to 7 elapsed hours, as recommended in Section 3.1.2, only about 0.5 h need be spent observing any calibrators (see Section 3.2). This leaves $t_{int} = 6.5$ h on target (Table 1, Col. 7). The in-beam calibrator must be strong enough to be well detected in a fringe-fit interval $\tau_{ff} = 60$ s (Table 1, Col. 5) with its poor associated baseline sensitivity ΔS^{128} (Table 1, Col. 6). That poor baseline sensitivity also leads to a poor image sensitivity (Table 1, Col. 8) despite the longer $t_{int} = 6.5$ h on target (Table 1, Col. 7).

3.2. Preparing Observing Schedules

Schedules for phase-referenced observations with the VLBA are usually prepared with SCHED. In the in-beam style, schedules are dominated by long target observations. In the nodding style, the schedules rapidly cycle between calibrator and target with a switching time τ_s. The following SCHED commands compactly define two elapsed hours for the nodding example with $\tau_s = 300$ s featured in Section 1:

```
source   = 'J1419+2706'  dur = 120  /
group    2 repeat 23
  source = 'NGC5548'     dur = 180  /
  source = 'J1419+2706'  dur = 120  /
```

Some other factors to keep in mind while scheduling are (Walker 1999b; Wrobel 1999):

- Include at least two observations, each lasting four or more minutes, of a fringe finder source, and ensure that the fringe finder is up at all antennas. Without these observations, if there are any problems at the correlator, debugging can be very difficult.
- Include at least one or two scans on an amplitude check source that is strong and has sufficiently simple structure to be easy to model or image. This source will be used to bring the amplitude calibration of all antennas and baseband channels to the same scale.
- Include a phase reference check source, which is a phase calibrator near the main phase calibrator that can be used to check the quality of the phasing on observation day. Select this check source from a SCHED RD plot, keeping in mind that if the selected source has a triangle symbol then its one-dimensional positional accuracy is better than $1 - 2$ mas and it can therefore be used as an astrometric check source.
- If doing spectral line observations, include a bandpass calibrator. Often this calibrator could also serve as the amplitude check source and/or the fringe finder.
- If doing linear polarization observations, obtain good parallactic angle coverage on a calibrator at every antenna to determine the instrumental polarization. The phase calibrator may serve for this. It is also possible that one observation of a simple unpolarized source will suffice. Also, observe some source or source component of known polarization to calibrate the polarization position angle.
- Allow occasional gaps of 2 minutes or more so that the tape systems can do readback checks of recorder health. One gap every hour or two is adequate.

3.3. Preparing for Correlation

Positions for correlation of targets and various kinds of calibrators, including phase calibrators, should all assume a coordinate equinox of 2000. By default, VLBA Operations staff will (1) draw all available positions from the VLBA source catalog and (2) draw all unavailable positions from your observing schedule. Action (1) can be modifid by providing clear instructions through the parameter corsrcs in the SCHED key file. For example, `corsrcs = 'from SCHED file only'` will cause all source positions to be drawn from the observing schedule. Target positions for correlation should be accurate to less than

$$500 \text{ mas} \times \frac{22}{\nu_{\rm GHz}},$$

where $\nu_{\rm GHz}$ is the observing frequency in GHz; if possible, it is desired that a target position be better than this by a factor of at least 3-5, to provide the best results (Ulvestad 1999a). Keep this accuracy in mind when you select the size of your phase-referenced image!

We thank Franco Tinarelli (IRA, Bologna) for providing all the plotting capabilities in SCHED. NRAO is a facility of the National Science Foundation operated under cooperative agreement by Associated Universities, Inc.

REFERENCES

Beasley, A. J., & Conway, J. E. 1995, in ASP Conf. Ser. 82, Very Long Baseline Interferometry and the VLBA, eds. J. A. Zensus, P. J. Diamond, & P. J. Napier (San Francisco: ASP), 327

Beasley, A. J., & Güdel, M. 2000, ApJ, 529, 961

Briggs, D. S., Schwab, F. R., & Sramek, R. A. 1999, in ASP Conf. Ser. 180, Synthesis Imaging in Radio Astronomy II, eds. G. B. Taylor, C. L. Carilli, & R. A. Perley (San Francisco: ASP), 127

Brisken, W. F., Benson, J. B., Beasley, A. J., Fomalont, E. B., Goss, W. M., & Thorsett, S. E. 2000, ApJ, submitted

Browne, I. W. A., Patnaik, A. R., Wilkinson, P. N., & Wrobel, J. M. 1998, MNRAS, 293, 257

Carilli, C. L., Carlstrom, J. E., & Holdaway, M. A. 1999, in ASP Conf. Ser. 180, Synthesis Imaging in Radio Astronomy II, eds. G. B. Taylor, C. L. Carilli, & R. A. Perley (San Francisco: ASP), 565

Chatterjee, S. 1999a, VLBA Scientific Memorandum 18 (Socorro: NRAO)

Chatterjee, S. 1999b, VLBA Scientific Memorandum 22 (Socorro: NRAO)

Condon, J. J. 1999, Proc. Natl. Acad. Sci. USA, 96, 4756

Fey, A. L., & Charlot, P. 1997, ApJS, 111, 95

Fomalont, E. B. 1995, in ASP Conf. Ser. 82, Very Long Baseline Interferometry and the VLBA, eds. J. A. Zensus, P. J. Diamond, & P. J. Napier (San Francisco: ASP), 363

Fomalont, E. B., Goss, W. M., Beasley, A. J., & Chatterjee, S. 1999, AJ, 117, 3025

Garrington, S. T., Garrett, M. A., & Polatidis, A. 1999, New Astronomy Reviews, 43, 629

Herrnstein, J. R., Greenhill, L. J., Moran, J. M., Diamond, P. J., Inoue, M., Nakai, N., & Miyoshi, M. 1998, ApJ, 497, L69

Kellermann, K. I., Vermeulen, R. C., Zensus, J. A., & Cohen, M. H. 1998, AJ, 115, 1295

Ma, C., et al. 1998, AJ, 116, 516

Niell, A. E. 1996, Journal of Geophysical Research, 101, 3227

Patnaik, A. R., Browne, I. W. A., Wilkinson, P. N., & Wrobel, J. M. 1992, MNRAS, 254, 655

Peck, A. B., & Beasley, A. J. 1998, in ASP Conf. Ser. 144, IAU Colloquium 164: Radio Emission from Galactic and Extragalactic Compact Sources, eds. J. A. Zensus, G. B. Taylor, & J. M. Wrobel (San Francisco: ASP), 155

Perley, R. A., & Erickson, W. C. 1984, VLA Scientific Memorandum 146 (Socorro: NRAO)

Perley, R. A., & Taylor, G. B. 1999, The VLA Calibrator Manual, NRAO user document

Reid, M. J. 1999, in ASP Conf. Ser. 180, Synthesis Imaging in Radio Astronomy II, eds. G. B. Taylor, C. L. Carilli, & R. A. Perley (San Francisco: ASP), 481

Reid, M. J., Readhead, A. C. S., Vermeulen, R. C., & Treuhaft, R. N. 1999, ApJ, 524, 816

Sovers, O. J., Fanselow, J. L., & Jacobs, C. S. 1998, Reviews of Modern Physics, 70, 1393

Taylor, G. B., Vermeulen, R. C., Readhead, A. C. S., Pearson, T. J., Henstock, D. R., & Wilkinson, P. N. 1996, ApJS, 107, 37

Taylor, G. B., Silver, C. S., Ulvestad, J. S., & Carilli, C. L. 1999a, ApJ, 519, 185

Taylor, G. B., Beasley, A. J., Frail, D. A., Kulkarni, S. R., & Reynolds, J. E. 1999b, A&AS, 138, 445

Thompson, A. R., Moran, J. M., & Swenson, G. W., Jr. 1986, Interferometry and Synthesis in Radio Astronomy (New York: John Wiley & Sons)

Treuhaft, R. N., & Lanyi, G. E. 1987, Radio Science, 22, 251

Ulvestad, J. S. 1999a, Novice's Guide to Using the VLBA, NRAO user document

Ulvestad, J. S. 1999b, VLBA Scientific Memorandum 20 (Socorro: NRAO)

Ulvestad, J. S. 2000, VLBA Scientific Memorandum 25 (Socorro: NRAO)

van Langevelde, H., Diamond, P. J., Vlemmings, W., Baudry, A., Habing, H. J., & Schilizzi, R. T. 1999, New Astronomy Reviews, 43, 575

Walker, R. C. 1999a, Accurate Source Position Service, NRAO user document

Walker, R. C. 1999b, in ASP Conf. Ser. 180, Synthesis Imaging in Radio Astronomy II, eds. G. B. Taylor, C. L. Carilli, & R. A. Perley (San Francisco: ASP), 433

Walker, R. C. 2000, The SCHED User Manual, NRAO user document

Walker, R. C., & Chatterjee, S. 1999, VLBA Scientific Memorandum 23 (Socorro: NRAO)

Wilkinson, P. N., Browne, I. W. A., Patnaik, A. R., Wrobel, J. M., & Sorathia, B. 1998, MNRAS, 300, 790

Wilson, B. D., Mannucci, A. J., & Edwards, C. D. 1995, Radio Science, 30, 639

Wrobel, J. M. 1999, The VLBA Observational Status Summary, NRAO user document

Wrobel, J. M. 2000, ApJ, 531, 716

Table 1. VLBA Parameters Related to Phase Referencing

ν (GHz) [1]	Θ_{FWHM} (′) [2]	τ_s (s) [3]	$\Delta\nu_{REC}^{128}$ (MHz) [4]	$\tau_{\rm ff}$ (s) [5]	ΔS^{128} (mJy) [6]	$t_{\rm int}$[a] (hours) [7]	$\Delta I_{\rm m}^{128}$ (μJy beam^{-1}) [8]	θ_{FWHM} (mas) [9]
0.33	126	...	32	60	50	6.5	380	22
0.33[b]	126	...	24	60	58	6.5	440	22
0.61[b]	67	...	8	60	100	6.5	760	12
1.4	29	300	32	120	4.7	3.5	69	5.0
1.7	25	300	32	120	4.8	3.5	69	4.3
2.3	18	300	32	120	5.2	3.5	76	3.2
2.3[c]	18	300	16	120	7.8	3.5	110	3.2
5.0	8	300	32	120	4.7	3.5	68	1.4
8.4	5	300	32	120	4.8	3.5	69	0.85
8.4[c]	5	300	16	120	8.9	3.5	130	0.85
15	3	120	32	60	12	3.5	130	0.47
22	2	60	32	30	31	3.5	230	0.32
43	1	30	32	15	69	3.5	360	0.17

[a]Assumes 7-h track with 0.5 h spent calibrating in in-beam style at $\nu < 1$ GHz and 3.5 h spent calibrating in nodding style at $\nu > 1$ GHz.

[b]Available simultaneously.

[c]Available simultaneously.

Table 2. Electronic Archives of VLBA and VLBI Visibility Amplitude Plots

Archive Name	ν (GHz)	Web Address	Ref.
VLBA Calibrator Survey	2.3, 8.4	http://magnolia.nrao.edu/vlba_calib/index.html	1
Radio Reference Frame Survey	2.3, 8.4	http://maia.usno.navy.mil/rorf/rrfid.html	2
Caltech-Jodrell Bank Surveys	1.7, 5.0	http://astro.caltech.edu/ tjp/cj	3
VLBA 2 cm Survey	15	http://www.cv.nrao.edu/2cmsurvey/	4

References. — (1) Peck & Beasley 1998; (2) Fey & Charlot 1997 and references therein; (3) Taylor et al. 1996 and references therein; (4) Kellermann et al. 1998

Fig. 1.— Example of the nodding style of phase referencing. *Top:* Calibrator J1419+2706 near target NGC 5548. *Bottom:* VLBA image at $\nu = 8.4$ GHz of the 2-mJy target NGC 5548, as phase referenced to the calibrator J1419+2706. The hatched ellipse shows the naturally-weighted synthesized beam at FWHM.

Fig. 2.— Example of the in-beam style of phase referencing. *Top:* Calibrator J1252+5634 near target Mrk 231. *Bottom:* VLBA image at $\nu = 0.33$ GHz of the 150-mJy target Mrk 231, as phase referenced to the calibrator J1252+5634. The filled circle shows the naturally-weighted and tapered synthesized beam at FWHM.

Fig. 3.— Example plots from the target planning tools available in the NRAO scheduling software SCHED.

Fig. 4.— Skyplot in a Hammer-Aitoff projection of 2700 *candidate* phase calibrators in the source catalog, dated 2000 April 17, in use at the VLBA correlator and distributed with SCHED.

Figure 1

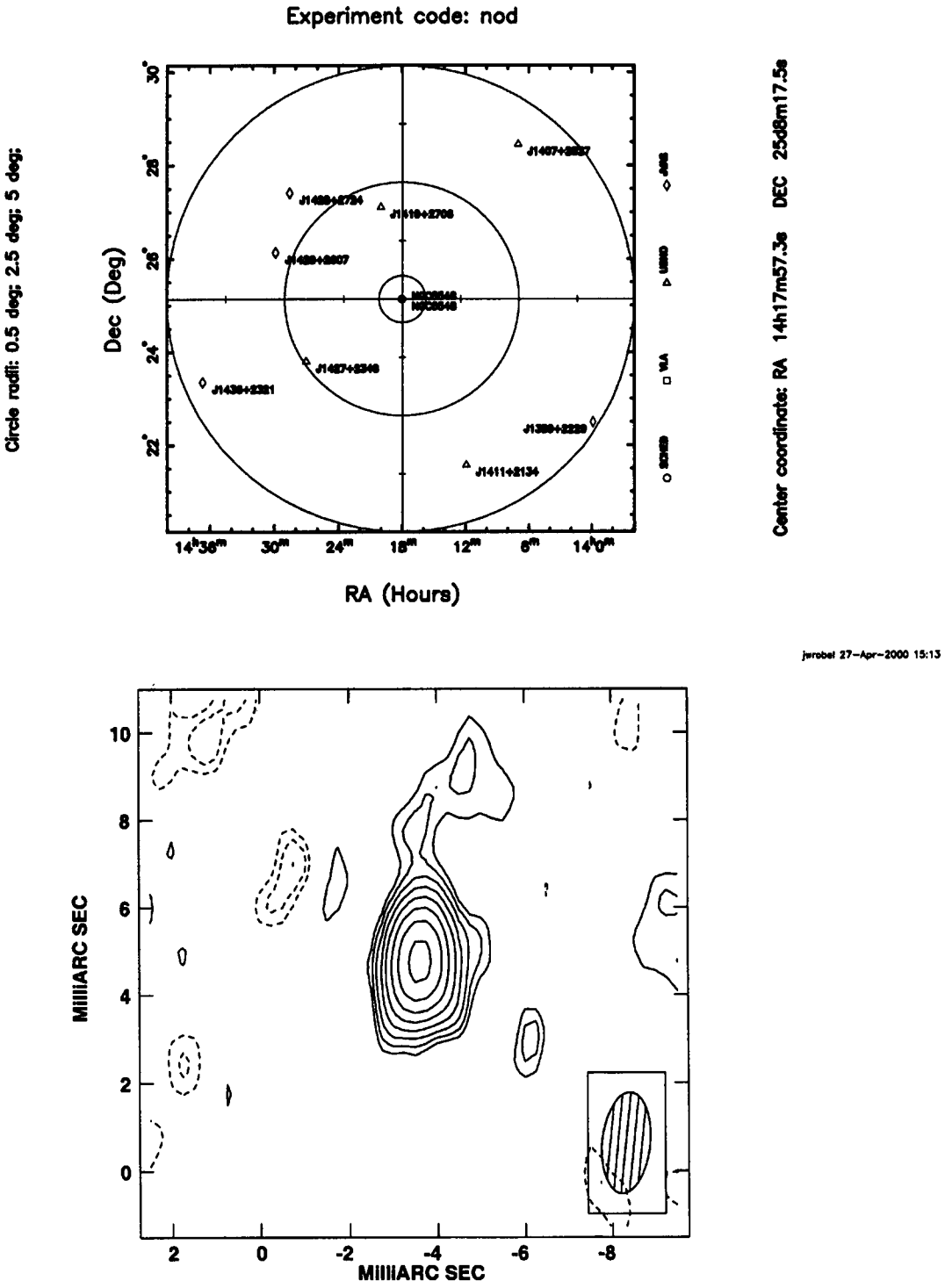
Experiment code: nod
Circle radii: 0.5 deg; 2.5 deg; 5 deg;
Center coordinate: RA 14h17m57.3s DEC 25d8m17.5s
Dec (Deg)
RA (Hours)
jwrobel 27-Apr-2000 15:13
MilliARC SEC
MilliARC SEC

Figure 2

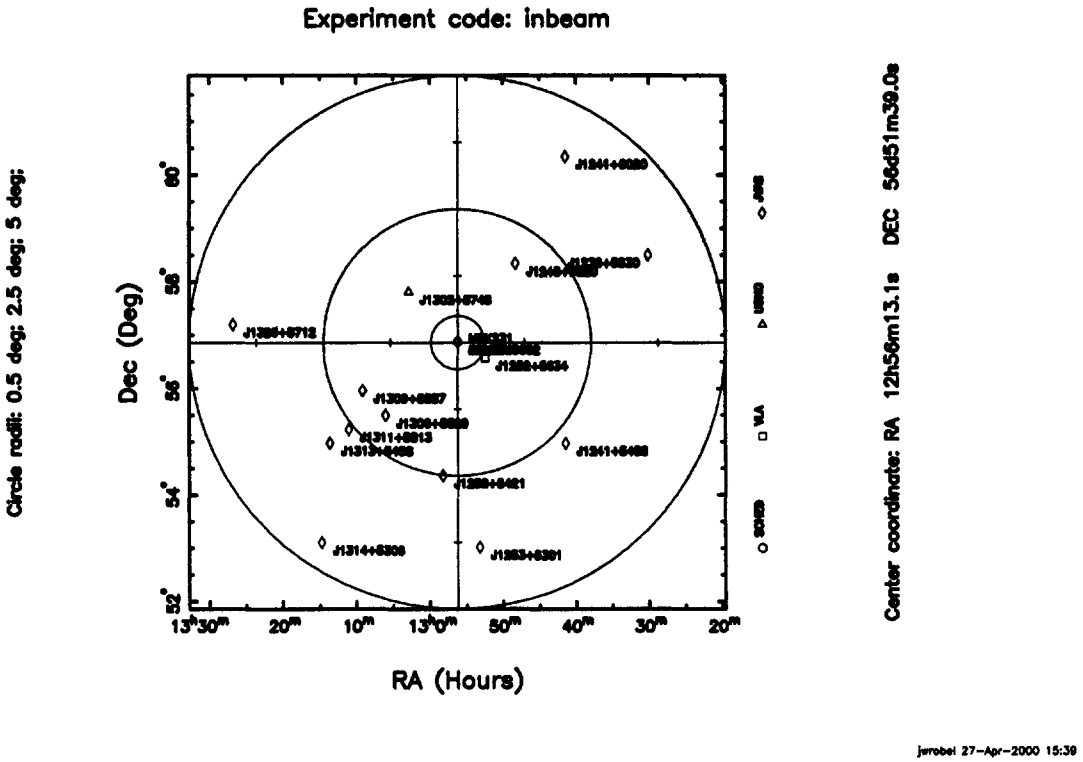
Experiment code: inbeam
Circle radii: 0.5 deg; 2.5 deg; 5 deg;
Center coordinate: RA 12h56m13.1s DEC 56d51m39.0s
Dec (Deg)
RA (Hours)
jwrobel 27-Apr-2000 15:39
Mrk231 327.974 MHz 20/06/98
Relative Decl. (mas)
Relative R.A. (mas)
100 pc

Figure 3

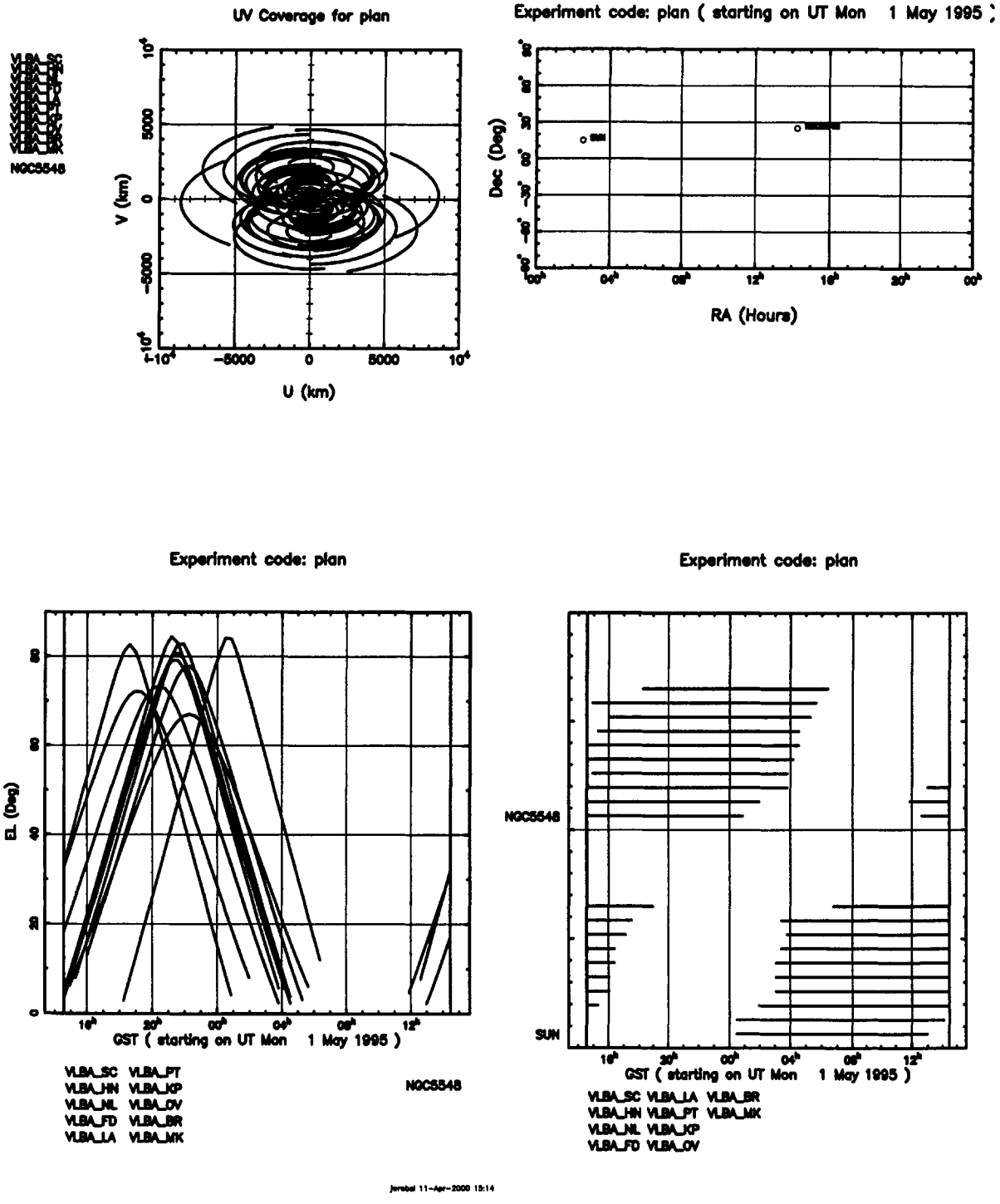
UV Coverage for plan
NGC5548
V (km)
U (km)
Experiment code: plan (starting on UT Mon 1 May 1995)
Dec (Deg)
RA (Hours)
Experiment code: plan
EL (Deg)
GST (starting on UT Mon 1 May 1995)
VLBA_SC VLBA_PT
VLBA_HN VLBA_KP
VLBA_NL VLBA_OV
VLBA_FD VLBA_BR
VLBA_LA VLBA_MK
NGC5548
Experiment code: plan
NGC5548
SUN
GST (starting on UT Mon 1 May 1995)
VLBA_SC VLBA_LA VLBA_BR
VLBA_HN VLBA_PT VLBA_MK
VLBA_NL VLBA_KP
VLBA_FD VLBA_OV
jvrobot 11-Apr-2000 15:14

Figure 4

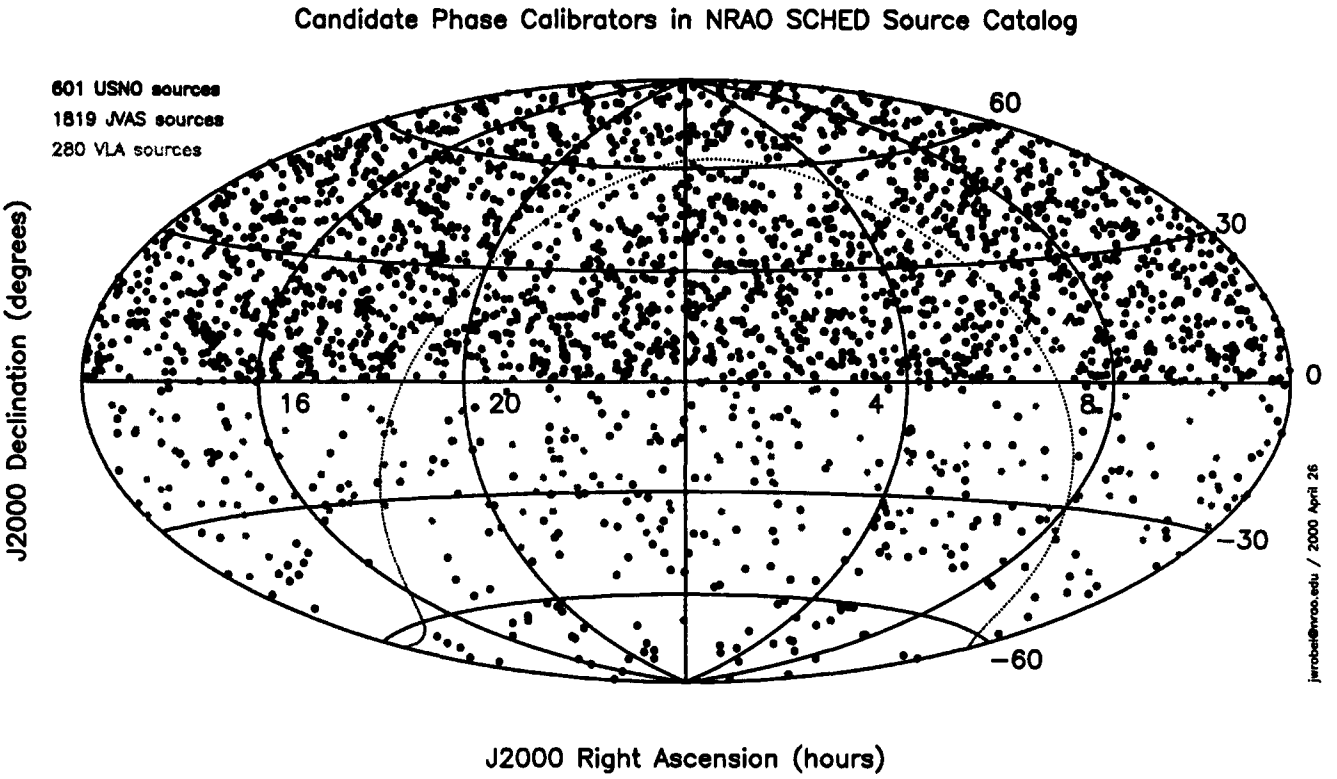
Candidate Phase Calibrators in NRAO SCHED Source Catalog
601 USNO sources
1819 JVAS sources
280 VLA sources
60
30
0
−30
−60
16
20
4
8
J2000 Declination (degrees)
J2000 Right Ascension (hours)
jmrobe@nrao.edu / 2000 April 26